Research Square

Preprints are preliminary reports that have not undergone peer review.
They should not be considered conclusive, used to inform clinical practice,
or referenced by the media as validated information.

Catalytic performance of Pd-Ni-Co/Al 2 O 3 catalysts in methane combustion

S. Todorova

todorova@ic.bas.bg

Institute of Catalysis Bulgarian Academy of Sciences

A. Naydenov

National Centre of Excellence Mechatronics and Clean Technologies"

D. Karashanova

Institute of Optical Materials and Technologies "Acad. Jordan Malinowski"

H. Kolev

Institute of Catalysis Bulgarian Academy of Sciences

I. Spassova

Institute of General and Inorganic Chemistry, Bulgarian Academy of Sciences,

Ralitsa Velinova

Institute of General and Inorganic Chemistry, Bulgarian Academy of Sciences,

Z. Geshkova

Institute of Catalysis Bulgarian Academy of Sciences

I. Yordanova

Institute of Catalysis Bulgarian Academy of Sciences

Ts. Parvanova-Mancheva

Institute of Catalysis Bulgarian Academy of Sciences

S. Delibaltova

Institute of Catalysis Bulgarian Academy of Sciences

K. Thenchev

Institute of General and Inorganic Chemistry, Bulgarian Academy of Sciences,

D. Moutafchieva

University of Chemical Technology and Metallurgy

P. Konova

Bulgarian Academy of Sciences

K. Tumbalova

Institute of General and Inorganic Chemistry, Bulgarian Academy of Sciences,

---

Research Article

Keywords:

Posted Date: November 11th, 2026

DOI: https://doi.org/10.21203/rs.3.rs-11394209/v1

License: This work is licensed under a Creative Commons Attribution 4.0 International License.
Read Full License

Additional Declarations: No competing interests reported.

Catalytic performance of Pd-Ni-Co/Al_2O_3 catalysts in methane combustion

S. Todorova[1,2*], A. Naydenov[2,3], D. Karashanova[4], H. Kolev[1], I. Spassova[2,3], Ralitsa Velinova[2,3], Z. Geshkova[1], I. Yordanova[1], Ts. Parvanova-Mancheva[1], S. Delibaltova[1], K. Thenchev[1], D. Moutafchieva[5], P. Konova[3], K. Tumbalova[2,3]

[1] Institute of Catalysis, Bulgarian Academy of Sciences, Acad. G. Bonchev St., Block 11,1113 Sofia, Bulgaria

[2] National Centre of Excellence Mechatronics and Clean Technologies", Sofia, 8 bul. Kliment Ohridski, Sofia, Bulgaria

[3]Institute of General and Inorganic Chemistry, Bulgarian Academy of Sciences, Acad. G. Bonchev St., Block 11,1113 Sofia, Bulgaria

[4] Institute of Optical Materials and Technologies "Acad. Jordan Malinowski", Bulgarian Academy of Sciences, Sofia, Bulgaria

[5] University of Chemical Technology and Metallurgy,8 Kliment Ohridski Blvd., Sofia, Bulgaria

[*]E-mail: todorova@ic.bas.bg

Abstract

Pd-based catalysts were prepared by successive wet impregnation of γ-Al_2O_3 with aqueous solutions of Ni, Co and Pd nitrates: Ni and Co were first co-deposited from a mixed solution, followed by Pd introduction in a second impregnation step. They were characterized by X-ray diffraction (XRD), X-ray photoelectron spectroscopy (XPS), temperature programmed reduction (TPR), temperature programmed oxidation (O_2-TPD), X-ray fluorescence measurements (XRF), BET method. The variation of the nickel content during the synthesis of the PdNix0.5Co/Al_2O_3 catalysts leads to the formation of different oxide phases on the surface. At nickel contents up to 1 wt%, the main phases are NiO weakly interacting with the support and $NiAl_2O_4$ and $CoAl_2O_4$. As the nickel content increases, strongly non-stoichiometric oxide phases appear, consisting of NiO moderately interacting with Al_2O_3 and mixed Ni–Al phases. Pd^0, Pd^{2+} and Pd^{4+} species are all observed on the surface of the catalysts calcined at 450 °C, whereas calcination of the cobalt- and nickel-modified support at 800 °C results in the formation of aluminate phases on the surface and the stabilisation of palladium as PdO. The highest activity of the catalyst containing 5 wt% Ni is very likely a result of the good contact of PdO with nickel aluminate and NiO. High-temperature calcination at 800 °C enhanced the catalytic activity of the catalyst with the lowest nickel content, owing to the increased amount of nickel aluminate on the surface.

Article Highlights

- Pd-Nix-0.5Co/Al_2O_3 catalyst successively synthesized by wet impregnation.
- NiO, $NiAl_2O_4$, $CoAl_2O_4$ and PdO phases identified

- At 5 wt% Ni the highest activity is due to the good contact of PdO with $NiAl_2O_4$ and NiO

Keywords: Methane, Emissions, Catalytic combustion, Pd–Co-Ni/alumina

1.Introduction

Achieving carbon neutrality requires substantial reductions in greenhouse gas emissions, with particular attention to methane (CH_4), the main component of natural gas [1, 2]. Although natural gas produces lower CO_2 emissions than coal and oil due to its higher H/C ratio and energy density, methane itself is a potent greenhouse gas with a significantly higher global warming potential than carbon dioxide [3, 4]. Consequently, reducing methane emissions has become a key priority in international climate policies.

Catalytic methane combustion is an effective approach for simultaneously mitigating methane emissions and producing useful energy. Compared with conventional thermal combustion, catalytic oxidation enables complete methane conversion at lower temperatures, resulting in higher energy efficiency and reduced emissions of harmful pollutants [5, 6]. This technology has attracted considerable interest in applications such as power generation, lean-burn gas turbines, catalytic combustors, and the treatment of ventilation air methane from coal mines and emissions from the oil and gas industry.

Methane accounts for approximately 14% of global greenhouse gas emissions, with major anthropogenic sources including agriculture, fossil fuel extraction, landfills, and wastewater treatment. Atmospheric methane concentrations have more than doubled since the pre-industrial era, making methane emission control one of the most effective short-term strategies for limiting global warming [7]. The United Nations Environment Programme director recently stated that "Cutting methane emissions is the best way to slow down climate changes over the next 25 years" [8]. According to the Global Energy Outlook 2019 report, 40 million tons of methane leaked from the coal mines in 2018, whereas 80 million tons were lost from the oil/gas industry. The researchers at the US Department of Energy's Lawrence Berkeley National Laboratory have demonstrated that methane causes an increasing greenhouse effect on the earth's surface. The special report of the Intergovernmental Panel on Climate Change (IPCC) indicates that a significant reduction in the non-CO2 greenhouse gases such as methane is necessary to keep the global warming below 1.5 or 2ºC [9]. According to recent estimates by the UN Environment Programme (UNEP) and the Climate and Clean Air Coalition (CCAC), methane emission reductions of 45% by 2030, based on available targeted measures and additional measures in line with the UN Sustainable Development Goals, could avoid 0.3ºC of global warming by 2045 [10].

The European Green Deal and Horizon Europe place strong emphasis on climate-neutral technologies and pollution reduction, supporting the development of advanced catalytic processes for greenhouse gas and volatile organic compound (VOC) abatement. Therefore, research on efficient catalysts for methane oxidation remains highly relevant for achieving future environmental and energy sustainability goals.

The methane combustion on model Pd catalysts has been studied extensively [3, 11-14] and some review articles have been published to summarize the development of catalysts for methane oxidation [13, 14].

In general, the activity of Pd in the reaction of methane oxidation depends on the metal particle size, morphology, and the interaction between Pd particles and the support. Most of the catalysts, designed for methane combustion, are based on palladium – separately or in combination with different metals or metal oxides, supported on alumina. The main problem in the practice is the deactivation of the Pd-based catalysts. Palladium catalysts are deactivated by

three main pathways: 1) sintering, 2) water adsorption and hydroxyls formation and 3) sulphate formation [4]. Therefore, it is very challenging to develop Pd supported materials with excellent activity and hydrothermal stability for methane combustion [15]. The problem could be tackled by using promotors and application of supports with new properties, as for example the nanostructured porous oxides. Promoters have been added to the Pd/Al_2O_3 catalyst to improve its performance. The efforts of all the researchers are focused on a development of new types of catalysts and optimization of the existing catalytic systems in order to prevent Pd sintering, providing at the same time sufficient activity at relatively low temperatures (below 500°C). However, because of the noble metals' high price the transition metal oxides (Ni, Cu, Mn, Co, Fe, Cr, etc.) have been considered as a good alternative in the practice as materials for synthesis of CH_4 combustion catalysts [16-19]. According to the literature data the most promising promoters are oxides of Ni, Mn, Co [20-23]. Co_3O_4, MnO_2 and NiO are p-type semiconductors characterized by low metal-oxygen bond energy and surface non-stoichiometry. These two features lead to the formation of surface oxygen vacancies, which is precondition for high catalytic activity [24].

Our previous studies have demonstrated that the activity and stability of Pd/Al_2O_3 catalysts for complete methane oxidation can be significantly improved by the addition of transition metal oxides, particularly Co, Ni, Ce and La promoters [25-32]. Among the investigated systems, Co-modified Pd catalysts exhibited the highest performance due to the stabilization of palladium in its active PdO state and the enhanced mobility of lattice oxygen. Experimental and theoretical studies confirmed that methane oxidation proceeds predominantly via a Mars–van Krevelen mechanism, in which catalyst reoxidation is the rate-determining step. The formation of spinel phases such as $CoAl_2O_4$ and $NiAl_2O_4$ was found to improve the thermal stability of PdO and catalyst durability, while Ce-containing catalysts promoted Pd reoxidation through the Ce^{4+}/Ce^{3+} redox cycle. These findings demonstrate that the nature of the promoter, its loading and the preparation method strongly influence the structure, redox properties and catalytic performance of Pd-based catalysts for methane combustion.

Co_3O_4 possesses a normal spinel structure, and its partial substitution with Ni^{2+} offers an effective strategy for improving catalytic activity through the synergistic interaction of the Co^{3+}/Co^{2+} and Ni^{3+}/Ni^{2+} redox couples [32,33]. Mixed spinel $NiAl_2O_4$ exhibits high structural and thermal stability, maintaining catalytic activity under harsh reaction conditions where single metal oxides tend to deactivate because of sintering or carbon deposition. Owing to its excellent redox properties, low cost and abundance of its constituent elements, $NiAl_2O_4$ has attracted considerable attention as an efficient catalyst for complete methane oxidation in the temperature range of 350-550°C, as well as for various electrochemical applications.

The synergistic interaction between Co and Ni in $NiAl_2O_4$ has been reported to enhance catalytic performance in methane oxidation through improved textural properties, high crystallite dispersion and increased surface oxygen mobility [34]. In Pd- $NiAl_2O_4$ catalysts, the intimate contact between Pd and the mixed oxide facilitates oxygen transfer from the support to palladium, promoting PdO regeneration and improving methane oxidation activity [35]. Furthermore, surface modification of amorphous SiO_2 with cobalt-nickel mixed oxides strengthens the interaction between Pd and the mixed oxide, resulting in significantly enhanced catalytic performance and lower methane light-off temperatures compared with the unmodified catalyst [35].

Considering all the above-mentioned background, and based on our previous results on the beneficial effect of Pd/Al_2O_3 catalysts modified with cobalt and nickel, this work proposes the design of highly active palladium catalysts doped with both Co and Ni elements.

2. Experimental

2.1. Catalysis preparation and characterization

The Pd-based catalysts were prepared by successive wet impregnation of γ- Al_2O_3 (Rhône-Poulenc, France) using aqueous solutions of nickel nitrate ($Ni(NO_3)_2 \cdot 6H_2O$), cobalt nitrate ($Co(NO_3)_2 \cdot 6H_2O$), and palladium nitrate ($Pd(NO_3)_2 \cdot 2H_2O$). Nickel and cobalt was first deposited onto the alumina support by mixed aqueous solution of Co and Ni nitrates, followed by calcination before introducing palladium in a second impregnation step. The catalysts contained a nominal Pd loading of 0.3 wt.%, while the nickel content was varied in the range of 0.25 weight percent to 15 wt%, and the cobalt content in all samples was 0.5%. The samples were calcined at 450ºC after each impregnation stage. To evaluate the effect of high-temperature calcination, additional samples were prepared using the catalysts with the lowest and the highest nickel contents. Following the deposition of the transition metal species, the samples were calcined according to a three-step procedure: 3 h at 300 °C, 2 h at 450 °C, and 4 h at 800 °C. Palladium was then deposited onto the pre-calcined samples, followed by a final calcination at 450 °C (samples denoted 15Ni+0.5Co (800)+0.2 Pd and 0.25Ni+0.5Co (800)+0.2 Pd).

Powder X-ray diffraction (XRD) patterns were recorded on a Bruker D8 Advance diffractometer equipped with Cu Kα radiation and a LynxEye detector over the 2θ range of 10-80°, using a step size of 0.02°. Phase identification was carried out with the X'Pert HighScore software.

The reducibility of the catalysts was investigated by H2 temperature-programmed reduction (H_2-TPR). Prior to the measurements, the samples were pretreated in flowing Ar at 150ºC for 1 h. The TPR experiments were performed in 10 vol.% H_2/Ar (10 mL min^{-1}) with a heating rate of 10ºC min^{-1} up to 700ºC.

The Oxygen temperature-programmed desorption (O_2-TPD) was carried out in micro reactor system Hiden CATLAB at atmospheric pressure with 0.150 g of sample (powder), reactor diameter 6 mm. Prior to O_2-TPD, the sample was pre-treated at 150ºC (heating rate 10ºC/min) for 30 min under Ar flow. The next temperature was increased to 400ºC (heating rate 10ºC/min) under 5 vol% O_2/Ar (flow rate 50 cm^3/min), for 60 min and were cooled to room temperature. The desorption step was conducted under Ar flow (50 cm^3/min) up to 950ºC at a heating rate 10ºC/min and the signal of O_2 (m/z = 32) were detected by the mass spectrometer QGA Hiden analytical.

The chemical composition of the Pd-based catalysts was determined by X-ray fluorescence measurements applying energy-dispersive X-ray fluorescence analyzer ED-XRF SPECTROSCOUT, XRF Analyzer Pro software v. 3.6, SPECTRO AMETEK Analytical Instruments GmbH.

The morphology, the microstructure and the phase composition of the catalysts were examined by transmission electron microscopy (TEM), in high-resolution transmission electron microscopy (HRTEM) and selected area electron diffraction (SAED) modes using a JEOL JEM 2100 microscope (JEOL Ltd., Tokyo, Japan) operated at an accelerating voltage of 200 kV. TEM and HRTEM images were collected at magnifications of 40,000× and 600,000×, respectively, while SAED patterns were acquired with a camera length of 250 mm.

The specific surface area, pore volume and pore size distribution of the supported catalyst samples were determined by low-temperature (77.4 K) nitrogen adsorption using a Quantachrome Nova 1200e apparatus. The specific surface area was determined according to the BET method. The pore size distribution was made by the Barrett-Joyner-Halenda (BJH) method, using the desorption branch of the isotherm. Total pore volume (V_t) and average pore diameter (D_{av}) were calculated according to the Gurvich rule at a relative pressure close to 0.99. The samples were degassed at 200°C for 18 hours.

X-ray photoelectron spectroscopy (XPS) measurements were performed on an ESCALAB MkII (VG Scientific) spectrometer operating under an ultrahigh vacuum of

approximately 5 × 10^{-10} $^{-}$9 mbar [M1.1]and equipped with a twin-anode Mg Kα/Al Kα X-ray source. Only Al Kα measurements are presented for these samples. The binding energy scale was referenced to the C 1s peak of adventitious carbon at 285.0 eV. Spectral processing included Shirley background subtraction [36], correction for X-ray satellite contributions, and peak fitting using mixed Gaussian-Lorentzian functions. Surface atomic concentrations were calculated from the normalized peak areas using the corresponding Scofield photoionization cross-sections [37].

2.2. Catalytic test

The catalytic activity of investigated catalysts was evaluated in the complete oxidation of methane in a continuous- flow type of reactor with a gaseous hourly space velocity (GHSV) of 100 000 h^{-1}.The inlet concentrations of the CH_4 were 950 ppm, while the oxygen concentration was 17.0 vol%. All gaseous mixtures were balanced to 100 vol% with nitrogen (4.0). The catalyst bed volume was 0.5 cm^3 (0.3 cm^3 catalyst and 0.2 cm^3 quartz-glass particles of the same size) and the reactor diameter of 6.0 mm ($D_{reactor}/D_{particles}\geq10$). The reaction temperature was maintained below 450°C, corresponding to the practical upper limit commonly applied in VOC abatement processes. Gas flow rates were precisely controlled using Bronkhorst mass flow controllers. The reaction products were continuously monitored in real time with a MultiGas FTIR gas analyzer (Model 2030G) produced by MKS Instruments Inc. (Andover), enabling quantitative measurement of VOCs, CO, CO_2, and H_2O.

3. Results and discussion

The chemical composition of the catalysts was determined by X-ray fluorescence (XRF, Table 1) analysis. The experimentally determined contents of Pd, Ni and Co were close to their nominal values, indicating that the impregnation procedure resulted in an efficient incorporation of the active components onto the Al_2O_3 support.

Table 1. Ni, Pd and Co content of the catalysts determined by X-ray fluorescence (XRF) analysis.

Catalyst	Ni (wt%)[a]	Pd (wt%) [a]	Co (wt%) [a]
0.2Pd**0.25Ni**0.5Co	0.213	0.2490	0.5510
0.2Pd**0.25Ni**0.5Co-800°C[b]	0.240	0.2550	0.5660
0.2Pd**0.5Ni**0.5Co	0.2884	0.3080	0.5667
0.2Pd**1Ni**0.5Co	1.212	0.2910	0.4731
0.2Pd**5Ni**0.5Co	4.784	0.3060	0.4450
0.2Pd**10Ni**0.5Co	10.12	0.3300	0.4979
0.2Pd**15Ni**0.5Co	11.03	0.3025	0.3809
0.2Pd**15Ni**0.5Co -800°C[b]	11.23	0.3703	0.5600

XRF analysis: SPECTRO (AMETEK) spectrometer, TQ Catalyst Powders method (20 mm cup), vacuum, 300 s.

[a]Mean of two measurements;

[b] Samples are calcined at 800°C after Co and Ni deposition.

Fig. 1 shows the nitrogen adsorption-desorption isotherms and the corresponding pore size distributions of the catalyst samples. Only the Ni loadings (wt%) are shown in the figure; the Pd and Co contents are given in Table 1. The isotherms of the Pd-Ni-Co samples with different Ni contents exhibit broadly similar profiles, with no substantial changes in their overall shape or hysteresis loops. The figure indicates that the isotherms belong to type IV according to the IUPAC classification which is associated with mesoporous materials [38].

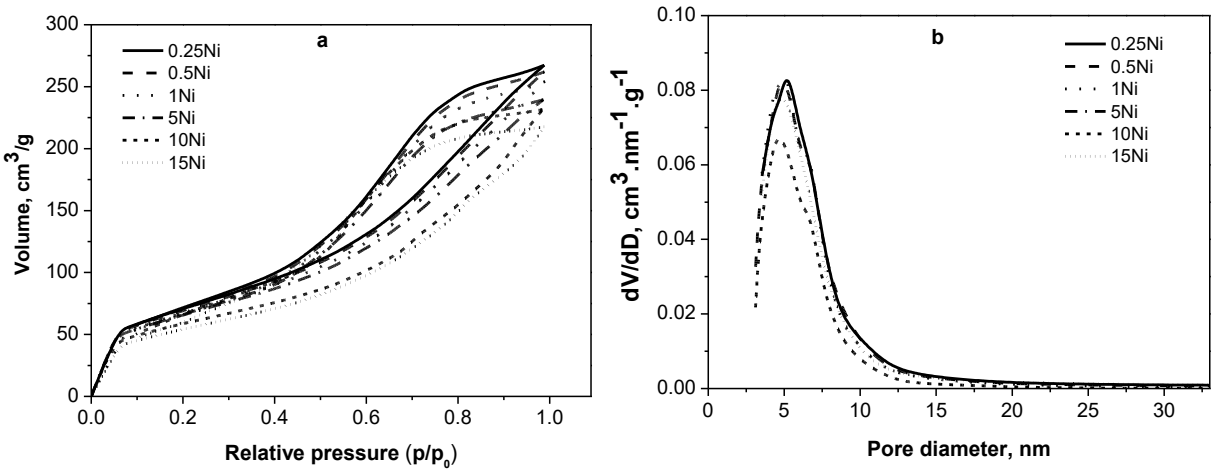


Figure 1. Nitrogen adsorption-desorption isotherms (a) and pore size distributions (b) of the studied samples.

The isotherms exhibit hysteresis loops characteristic of mesoporous materials. The observed H2- type hysteresis is associated with complex pore networks in which pore blocking, percolation effects, and sometimes cavitation may influence the desorption process. Such behaviour is consistent with a non-uniform pore structure that may include ink-bottle shaped pores. However, the precise pore geometry cannot be established from the hysteresis loop alone.

Nevertheless, differences in the textural parameters are observed as the Ni content increases. Both the specific surface area and total pore volume decrease, from 260 to 196 m^2/g and from 0.42 to 0.34 cm^3/g, respectively, whereas the average pore diameter increases slightly (Table 2). These changes may be associated with modifications in the pore structure and/or partial blockage of accessible pores by Ni-containing species. These results suggest that increasing Ni content may affect the porous structure, potentially through pore blocking, changes in the pore network, or structural modifications during synthesis.

Table 2. Textural characteristics of samples: BET specific surface area, total pore volume, and average pore diameter of prepared catalysts.

Sample	S_{BET}, m^2/g	V_t, cm^3/g	D_{av}, nm
0.2Pd **0.25 Ni** 0.5Co	260	0.42	6.4
0.2Pd **0.5 Ni** 0.5Co	254	0.41	6.4
0.2Pd **1 Ni** 0.5Co	245	0.39	6.4
0.2Pd **5 Ni** 0.5Co	240	0.37	6.2
0.2Pd **10 Ni** 0.5Co	212	0.36	6.8
0.2Pd **15 Ni** 0.5Co	196	0.34	7.0

XRD pattern of the synthesized catalysts (Fig. 2) show the presence of γ- Al_2O_3 (PDF 00-001-1303), NiO (PDF 00-044-1159) and $NiAl_2O_4$ (PDF 00-001-1299). The reflections of $CoAl_2O_4$ and $NiAl_2O_4$ overlap, but the distinct reflection observed at 19.5° provides clear evidence for the formation of $NiAl_2O_4$ in all the catalysts. The presence of $CoAl_2O_4$ and $NiAl_2O_4$ is further confirmed by the HRTEM analysis, as shown below. For all the investigated samples, a very weak diffraction reflection is observed at 2θ= 42.82°, which could initially be attributed to the formation of $CoNiO_4$ oxide (PDF 00-010-0188). However, this region may also correspond to a reflection of NiO. Considering that the presence of NiO has been confirmed by TEM, it is much more likely that this reflection can be assigned to nickel oxide. No diffraction peaks attributable to cobalt oxides, metallic palladium, or palladium oxide were observed, indicating the high dispersion of palladium on the catalyst surface. These results further suggest that the oxide species are finely dispersed over the catalyst surface. The formations of the oxide surface phases in the present study are with accordance with the literature data's. Evidence for the simultaneous formation of Ni- and Co-containing oxide and aluminate species has also been reported for bimetallic Ni–Co/ Al_2O_3 catalysts. Siang et al. [39] prepared Ni–Co/Al_2O_3 catalysts using $Ni(NO_3)_2$ and $Co(NO_3)_2$ precursors and reported the coexistence of NiO, Co_3O_4, $NiAl_2O_4$ and $CoAl_2O_4$ species after calcination. Importantly, this demonstrates that simultaneous deposition of Ni and Co does not necessarily result in the formation of a single homogeneous Ni-Co oxide phase. Instead, Ni-Co interaction and metal-alumina interaction may occur simultaneously. In the study [40], where Ni-Co/γ-Al_2O_3 catalysts were prepared by simultaneous impregnation using $Ni(NO_3)_26H_2O$ and $Co(NO_3)_26H_2O$, followed by drying and calcination at 400ºC. The Ni loading was varied over a relatively broad range, while Co was simultaneously introduced from the same solution. The results demonstrate that the co-impregnation procedure can produce highly dispersed Ni and Co species interacting with the alumina support.

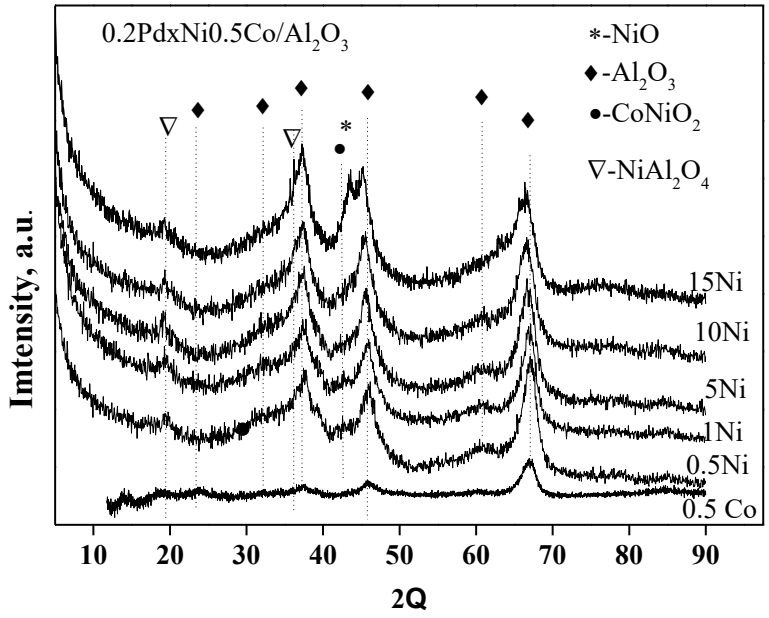


Figure 2. XRD patterns of studied catalysts after calcination at 450 °C

The reduction behaviour of the catalysts was investigated by H_2 temperature-programmed reduction (H_2-TPR).

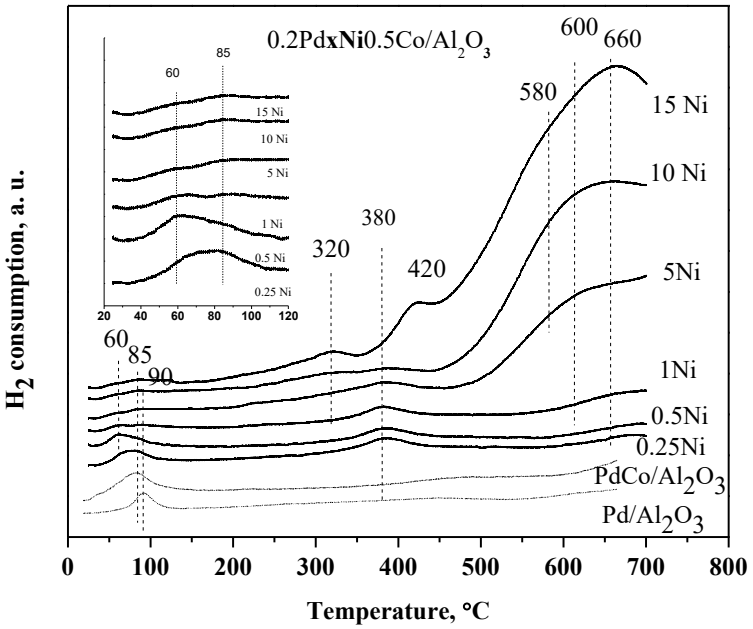


Figure 3. TPR profiles of all samples after calcination

The catalysts show hydrogen uptake in several temperature ranges: 50-100ºC, 300-400ºC, 400-600ºC and above 600ºC. The TPR profile of the Pd/Al_2O_3 catalyst shows a reduction maximum at 90 °C, which can be attributed to the reduction of PdO species strongly interacting with the support [29]. The addition only of the cobalt moves this peak to the lower reduction temperature, revealing the decreases in the interaction of PdO with the support. Simultaneous modification with Ni and Co results in the appearance of two reduction maxima in this temperature range, at 60 and 85ºC, which could be assigned to the reduction of two different PdOx species. The peak at 60ºC can be associated with highly dispersed and weakly interacting PdOx species, whereas the higher-temperature peak at 85ºC may originate from PdOx species with stronger interaction with the support. [41,42]. Based on this observation, it can be said that the addition of a transition metal oxide modulates the interaction of the PdO_x particles with the support surface and the simultaneous modification with cobalt and nickel leads to the formation of finely dispersed PdO particles that interact only weakly with the support.

It is usually accepted that reduction peaks appearing between 250 and 600ºC originate from NiO whose interaction with the support varies in strength. Peaks in the 250-400ºC range are commonly assigned to NiO that interacts only weakly with the support, whereas reduction at higher temperatures, but still below 600ºC, points to NiO species that interact moderately with Al_2O_3 [43]. Taking into account these statements, the reduction peak centred at 380ºC is most likely associated with the reduction of finely dispersed NiO species weakly interacting with the support. Bulk NiO is typically reduced at around 400ºC [44]. The shift of the reduction peak toward lower temperatures (to 320ºC for 15Ni) with increasing Ni content can be attributed to the NiO particles with limited interaction with Al_2O_3. According to the literature, the hydrogen consumption at 420 and 580ºC is ascribed to the reduction NiO with a different but moderate interaction with Al_2O_3 [44,45] and the hydrogen uptake in the interval 600-800ºC is attributed to the reduction of Ni^{2+} in mixed Ni-Al oxide phases strongly interacting surface [43,45]. At temperatures above 800ºC, the reduction is mainly attributed to crystalline $NiAl_2O_4$

spinel. At temperatures above 500°C, the reduction of surface cobalt species interacting strongly with the alumina support and/or cobalt aluminate-like phases [46,47] can may take place also. As evidenced by the TEM images, the Co-aluminate coexists with the nickel aluminate phase on the catalytic surface.

The O_2-TPD profiles of the 0.2Pd*x*Ni0.5Co/Al_2O_3 catalysts (x = 0.25-15 wt% Ni) and the reference samples are shown in Fig. 4. According to XRD, NiO is the predominant crystalline phase in the catalysts with 5-15 wt% Ni. In contrast, Ni in the low-loaded samples is expected to be highly dispersed or incorporated into the alumina as nickel aluminate.

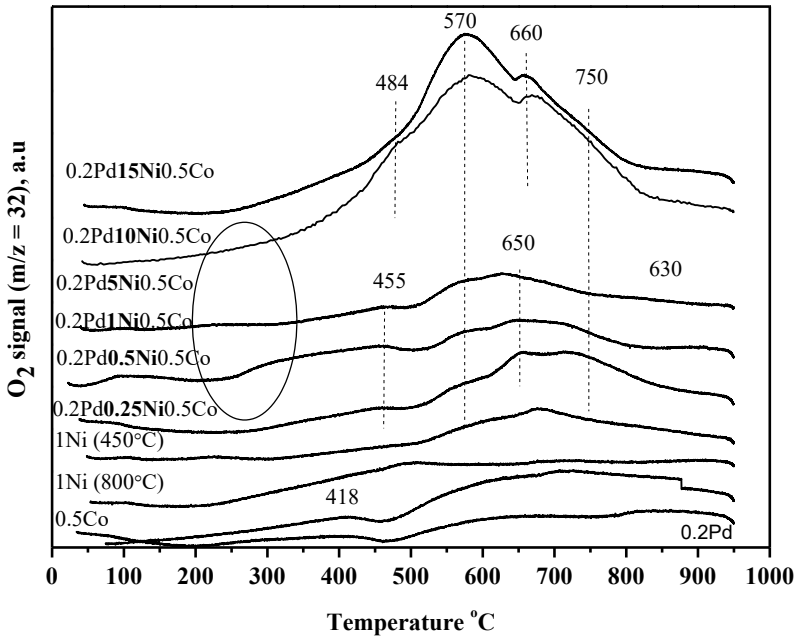


Figure 4. O_2-TPD profiles of the 0.2Pd*x*Ni0.5Co/Al_2O_3 catalysts and the reference samples. The profiles are offset vertically for clarity

The catalysts with higher Ni loadings (5–15 wt% Ni) released the largest amount of oxygen. Desorption started at ~150 °C with a very broad desorption peak in the range 200–300°C for the samples with Ni up to 5%, shoulder at 484 °C, reached a dominant maximum at 570°C, and was followed by a second, narrower peak at 660°C and a shoulder at 750°C. Chen et al. [48] identified the presence of two types of non-stoichiometric oxygen species on bulk NiO calcined at 500°C, denoted as α and β oxygen. The α species were associated with oxygen desorption in the 300-450 °C range, whereas the β species desorbed at higher temperatures, between 450 and 620°C. The low-temperature α species were attributed to mobile, extra-lattice oxygen predominantly associated with adsorbed oxygen species, while the high-temperature β species were assigned to lattice oxygen. In an earlier study, Seiyama and co-workers [49] proposed a more detailed classification based on four oxygen desorption peaks, designated α, β, γ, and δ, occurring over a temperature range of approximately 300–600 °C. The α and β peaks were tentatively assigned to molecular oxygen species, including physisorbed O_2 and O_2^-, whereas the γ and δ peaks were attributed to O^- species adsorbed on two distinct types of surface sites. For the NiO sample, pretreated at 500 °C, two oxygen-desorption peaks were observed, at approximately 300–450 °C and 450–620 °C, respectively [48]. These features were tentatively assigned to non-stoichiometric or mobile oxygen species associated with NiO, rather

than to lattice oxygen, since the latter is generally expected to be released only at temperatures above approximately 700 °C. In a separate experiment, the NiO sample was subjected to a thermal treatment at 700 °C prior to the TPD measurement. Only a small at oxygen peak was detected over the sample treated at 700 °C. Obviously, the amount of nonstoichiometric oxygen species is closely related to the pretreatment temperature, i.e. the higher the pretreatment temperature, the smaller the amount of nonstoichiometric oxygen species. The amount of nonstoichiometric oxygen in nickel oxide is closely related to the oxidation state of nickel, and it decreases with increasing preparation temperature [50].

Accordingly, the statement above and the fact that our samples are calcined at 450°C, the peaks at 418, 455 and 484 °C shoulder is assigned to oxygen adsorbed on Ni at the NiO surface. The intense peak at 570 °C and oxygen desorption at 630-660 °C could be assigned to non-stoichiometric or mobile oxygen species associated with NiO or Ni-Al surface phases. The shoulder at 750 °C is attributed to oxygen diffusing from deeper layers. The large desorption from the 5–15Ni catalysts therefore indicate that oxides on the surface are strongly non-stoichiometric, which is probably caused by the low calcination temperature.

The reference 1Ni (450 °C) sample exhibited a moderate oxygen-desorption peak at approximately 680 °C, which may be associated with non-stoichiometric oxygen species retained after the lower-temperature calcination treatment as was shown above. In contrast, the very week desorption peak at around 500 °C observed for the 1Ni (800 °C) sample may be related to the lower concentration of oxygen species available for desorption, because the $NiAl_2O_4$ spinel formation. A very broad desorption peak in the range 200–300 °C could be result of chemisorbed oxygen [51].

Among the reference samples, $0.5Co/Al_2O_3$ showed a weak α-oxygen peak at 418 °C and a broad band at ~710–750 °C from $Co_3O_4 \rightarrow CoO$; O_2 evolution from bulk Co_3O_4 and Co/CeO_2 has been reported to begin at ~750 °C [52].

The oxidation states of palladium, cobalt and nickel on the catalyst surface were determined by X-ray photoelectron spectroscopy (XPS) (Table 3 and Fig.5). Figure 5a presents the Pd 3d XPS spectra of the catalysts calcined at 450 °C. The binding energies in the range of 335.1–335.7 eV observed in the $Pd–Co/Ni/Al_2O_3$ catalysts are assigned to metallic palladium (Pd^0). Binding energies between 336.2 and 336.9 eV indicate the presence of PdO (Pd^{2+}) in all investigated samples. In addition, a third component was detected at 339.1 eV. This peak can be assigned to Pd^{4+} species, most likely associated with PdO_2 [25,26].

Table 3. Surface atomic concentrations (at.%) of the elements determined by X-ray photoelectron spectroscopy (XPS).

Catalyst	O 1s	Al 2p	Pd 3d			Co $2p_{1/2}$		Ni $2p_{3/2}$
			Pd^0	Pd^{2+}	Pd^{4+}	Co^{3+}	Co^{2+}	Ni^{2+}, Ni in oxide
0.2Pd**0.25Ni**0.5Co	59.46	34.47	0.36	2.61	0.29	0.94	1.14	0.69
0.2Pd**0.5Ni**0.5Co	59.15	35.37	0.32	2.33	0.26	0.72	0.38	1.47
0.2Pd**1Ni**0.5Co	60.72	34.38	0.25	2.49	0.37	0.33	0.10	1.35
0.2Pd**5N**i0.5Co	59.74	34.44	0.41	2.57	0.45	–	-	2.11
0.2Pd**10Ni**0.5Co	59.04	32.08	0.74	3.45	0.47	–	-	3.67
0.2Pd**15Ni**0.5Co	59.74	30.94	0.55	2.58	0.35	–	-	5.46

[a] surface Pd concentration on the Ni loading with the same Ni concentration according to our previous publication [31]

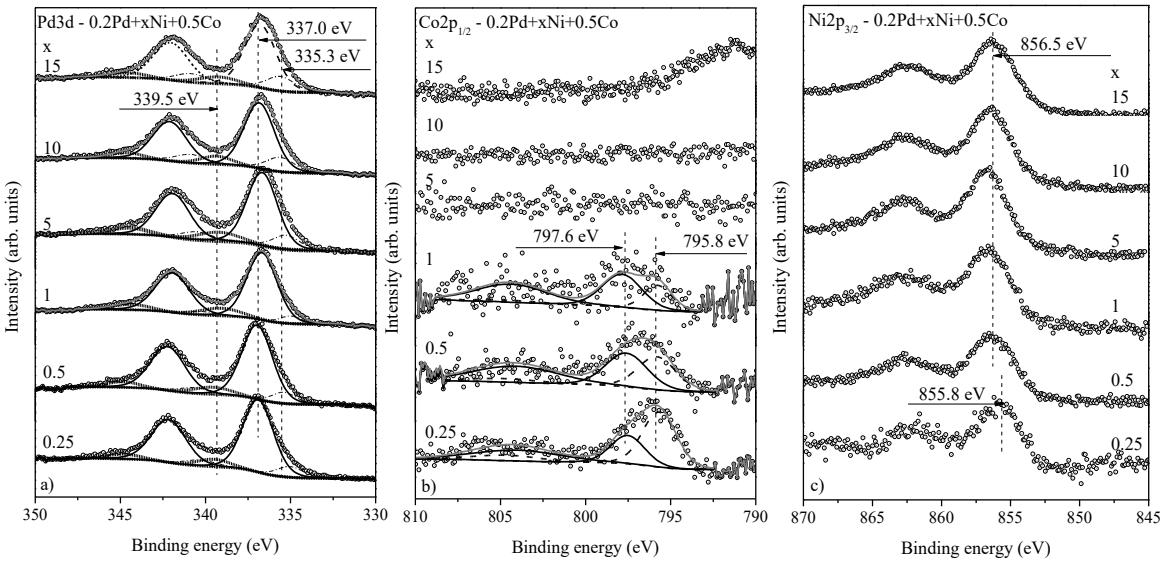


Figure 5. Pd 3d (a), Co 2p (b) and Ni2p (c) XPS spectra of Pdx% Ni0.5Co /Al_2O_3 catalyst after calcination at 450 °C. The empty circles represent the experimental data points in all figures. In Fig. 5a, Pd^{2+} fit is presented through a straight line, the Pd^0 fit – through the vertical dashes and the dash-dot fit represents Pd^{4+}. In Fig. 5b, the straight line represents Co^{2+}, and the dashed line represents Co^{3+}, both with their respective satellite features.

Deconvolution of the XPS spectra revealed that both Co^{2+} and Co^{3+} species are present on the surface of the catalysts containing up to 1 wt.% Ni, with Co^{2+} being the predominant oxidation state. In contrast, for the catalysts containing 5, 10, and 15 wt.% Ni, no Co 2p signals could be identified. This is most likely due to the coverage of the cobalt species by nickel, which prevents the detection of cobalt by the surface-sensitive XPS technique.

The Ni $2p_{3/2}$ spectrum exhibits components at 855.8 eV for sample with 0.25% Ni and 856.2–856.5 eV for other catalysts, accompanied by shake-up satellite feature at 861.6 -862.7 eV, characteristic of Ni^{2+} species. The observed binding energies are consistent with the coexistence of NiO and $NiAl_2O_4$ phases. The assignment is therefore supported by the XRD and TEM results [31,53,54].

As can be seen from Table 3, at low Ni content the Ni $2p_{3/2}$ peak appears at a binding energy of 855.8 eV. With increasing nickel content, this peak shifts to higher binding energies, reaching a maximum at 5% Ni, after which the binding energy decreases. The band close to 854.4 ± 0.3 eV is associated with NiO [55,56], while the band located between 856 and 857 eV is assigned to Ni^{2+} ions in the lattice of the $NiAl_2O_4$ phase [57]. According to H_2-TPR, finely dispersed NiO predominates in the sample with 0.25% Ni (Fig. 3). With increasing nickel content up to 5%, the proportion of mixed Ni–Al oxide phases (hydrogen uptake above 600 °C) increases, which accounts for the shift of Ni $2p_{3/2}$ to higher binding energies. The subsequent decrease of the binding energy at higher Ni contents is most likely due to the formation of NiO that interacts only weakly with the support, as evidenced by the H_2-TPR reduction peak at 320 °C assigned to such NiO (Fig. 3). The spectra of all analysed samples exhibit a typical shake-up satellite peak close to 861.8 ± 0.5 eV. For the samples calcined at 800 °C, Ni $2p_{3/2}$ is located

at a higher binding energy of 856.5 eV (Table 3 and Fig 5c), which is consistent with the formation of nickel aluminate. Additional evidence is the colour of the samples, which is blue to blue-green.

With increasing Ni content in the catalysts simultaneously modified with Co and Ni, the XPS results reveal a gradual increase in the surface concentration of Pd. In our previous studies on Pd–Ni/Al_2O_3 catalysts, no significant dependence of the surface Pd concentration on the Ni loading was observed [31]. In contrast, comparison of catalysts with identical Ni contents, but additionally modified with Co, demonstrates that the introduction of Co as a promoter into the Pd–Ni/Al_2O_3 system results in a pronounced increase in the surface concentration of Pd. The Pd surface concentrations determined in our previous study for the corresponding Pd–Ni/Al_2O_3 catalysts are given in parentheses in the table in black font.

XPS spectra of the samples calcined at 800 °C after Co and Ni deposition are shown in the Table 4 and Fig. 6.

Table 4. XPS binding energies (BE) and surface atomic concentrations of the 0.2Pd0.25Ni0.5Co and 0.2Pd15Ni0.5Co catalysts treated at 800 °C

Catalyst	O 1s lattice	O 1s non-lattice	Al 2p	Pd 3d	Co $2p_{3/2}$	Ni $2p_{3/2}$
0.2Pd0.25Ni0.5Co-800 °C	50.43	-	41.02	0.17	0.35	0.15
0.2Pd15Ni0.5Co-800 °C	48.85	9.44	37.16	0.08	0.23	4.23

Figure 6a presents the Pd 3d XPS spectra of the samples calcined at 800 °C. Pd 3d is weak due to the low Pd concentrations in the samples. Nevertheless, it can be seen that Pd is in the 2+ oxidation state in all samples [58]. It should be noted that the presence of metallic Pd cannot be excluded. However, due to the signal-to-noise ratio, it cannot be confirmed. In any case, the majority of Pd on the surface is in oxide form. The Pd $3d_{5/2}$ binding energy of the Pd^{2+} component depends on the calcination temperature of the Ni–Al_2O_3 support. On the support calcined at 450 °C it appears at 336.9 eV (Table 3), whereas on the support calcined at 800 °C it is observed at 336.1 eV, close to the value usually assigned to bulk PdO (Table 4). The higher binding energy at 450 °C indicates a more electron-deficient Pd^{2+} species, which we attribute to Pd–O–Ni interfacial contact between PdO and NiO. Similar Ni^{2+}–O–Pd interfaces, with electron transfer from Pd to Ni^{2+} across the bridging oxygen, have been reported for Pd/$Ni(OH)_2$ [59], and a positive Pd 3d shift caused by electron withdrawal by neighbouring Ni^{2+} has been described for Pd–NiO_x/TiO_2 [60]. After calcination of the support at 800 °C, Ni^{2+} is largely incorporated into the alumina lattice as $NiAl_2O_4$ [61], as indicated by the Ni $2p_{3/2}$ shift from 855.8 to 856.5 eV, so that little free NiO remains for Pd–O–Ni contact; PdO then interacts mainly with the spinel/alumina surface and its binding energy approaches that of bulk PdO.

The Co2p (Fig. 6b) spectra display two distinct main peaks, Co $2p_{3/2}$ at 781.8 eV and Co $2p_{1/2}$ at 797.5 eV, along with a 3d → 4s shake-up satellites at about 788 eV and 804 eV, respectively. Together, these features are characteristic of Co^{2+}. Co(II) can be identified by the satellite located 6.0–6.5 eV above the main $2p_{3/2}$ line [62]. Additionally, the spin-orbit splitting between the Co $2p_{3/2}$ and Co $2p_{1/2}$ levels also depends on the oxidation state and therefore serves as a diagnostic parameter. The observed splitting of approximately 15.8 eV [63] is consistent with Co^{2+} surface species.

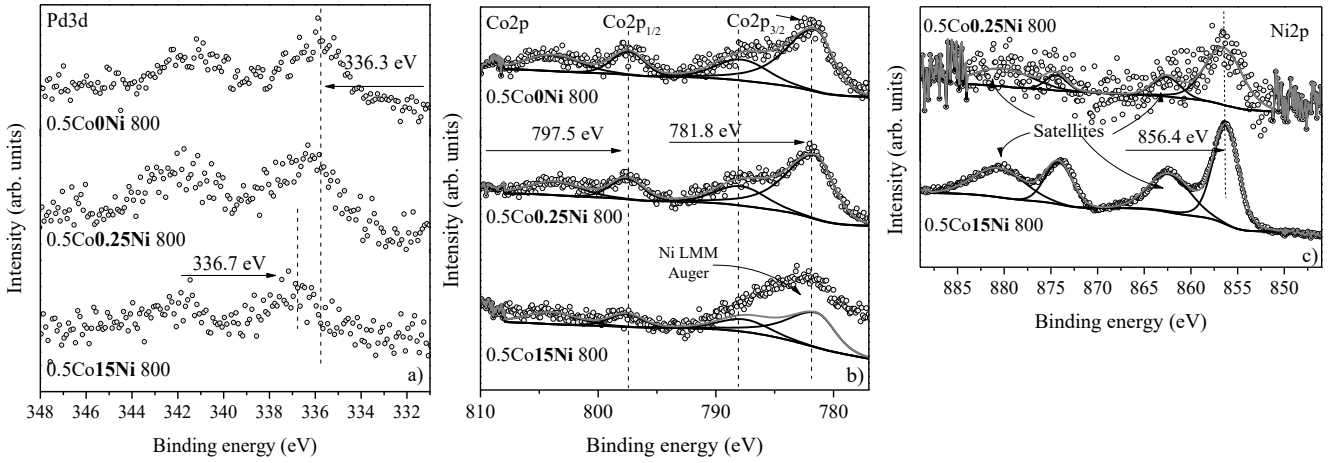


Figure 6. Pd 3d (a), Co 2p (b) and Ni2p (c) XPS spectra of PdxNi0.5Co /Al_2O_3 catalyst after calcination at 800 °C of the precursors xNi0.5Co/Al_2O_3 before Pd deposition. Both Co $2p_{3/2}$ and Co $2p_{1/2}$ are analyzed due to the weak signal of the Co $2p_{1/2}$ and the Ni LMM Auger overlap with Co $2p_{3/2}$.

The morphology of the catalyst containing 0.2 wt% Pd, 0.25 wt% Ni, and 0.5 wt% Co is shown in Fig. 7a) at 40,000× magnification and in Fig. 7c) and e) at 600,000× magnification. The images at the higher magnification reveal individual particles – typical for the Al_2O_3 support (Fig. 7c), for the metallic Pd, and the formed phases NiO and $CoAl_2O_4$ (Fig. 7d)). This differentiation is made possible due to the different electron contrast exhibited by Al_2O_3, metallic Pd, and the Co- and Ni-containing oxides particles. It can be seen also that the Al_2O_3 particles possess a characteristic elongated shape, whereas the metallic and oxide particles are nearly spherical, smaller than 10 nm in size, and distributed relatively uniformly across the surface of the support particles - a finding supported by XPS measurements. The phase composition of the sample is presented in Fig. 7b). Based on measured interplanar distances and the indexing of the polycrystalline diffraction pattern, the presence of gamma–Al_2O_3 and mixed oxide phases was identified. The presence of Pd and NiO is confirmed by the high resolution images, which also prove and the Al_2O_3 and $CoAl_2O_4$ phases.

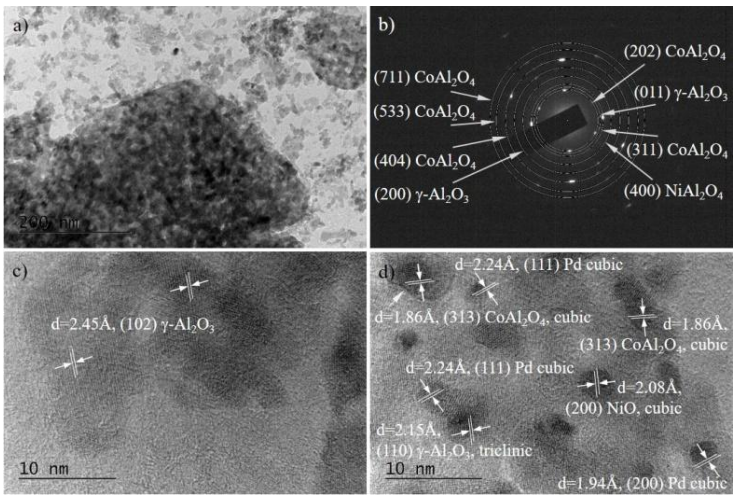


Figure 7. Bright field TEM micrograph (a), Selected area electron diffraction pattern (b) and High resolution TEM images (c, d) of Pd0.2Ni0.25Co0.5/γ-Al_2O_3 catalyst.

The catalytic performance of the mono- and bimetallic catalysts for complete methane oxidation as a function of reaction temperature is presented in Fig. 8. Complete oxidation of methane yielded only CO_2 and H_2O as reaction products over all investigated catalysts. For comparison, the activity of the Co-only modified sample ($Pd+Co/Al_2O_3$), calcined under the same conditions, is also shown in the figure. The modification of Pd/Al_2O_3 with different amounts of Ni and 0.5 wt.% Co demonstrated that the catalysts containing 5 wt.% Ni exhibited the highest activity. The activity order is as follow: 5%Ni>0.5Ni>10Ni>15Ni>1Ni>0.25Ni.

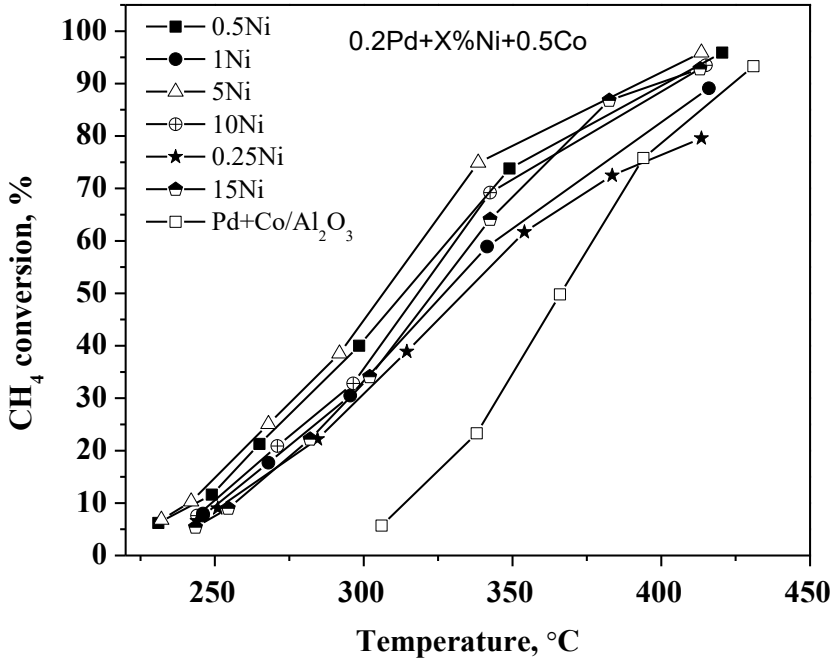


Figure 8. Temperature dependence of methane conversion during complete methane oxidation over $PdxNi0.5Co/Al_2O_3$ catalysts.

Our previous studies demonstrated that the modification of Pd/Al_2O_3 catalysts with different nickel loadings resulted in enhanced catalytic activity for methane oxidation, with the improvement being essentially independent of the nickel content. In the present work, the simultaneous incorporation of cobalt leads to a further enhancement of the catalytic performance compared with both the catalyst modified only with cobalt and the series containing different nickel loadings. Specifically, the temperature required to achieve 50% methane conversion (T_{50}) decreases from 320 °C for the Ni-modified catalysts [31] to 306 °C after the additional incorporation of cobalt, indicating a beneficial synergistic interaction between nickel and cobalt in promoting the catalytic activity of the Pd-based systems. One possible explanation for the higher activity of the catalysts modified simultaneously with nickel and cobalt, compared with those modified with nickel only [31], is the higher Pd dispersion (XPS data) in the Pd-Ni-Co catalysts.

As indicated above, the catalyst containing 5 wt% nickel ($0.2Pd5Ni0.5Co/Al_2O_3$) exhibited the highest activity. The literature data show that both NiO and $NiAl_2O_4$ promote methane oxidation over palladium catalysts [64–67]. Li et. Al. [64] proposed mechanism, according wich Pd incorporation distorts the NiO lattice and enhances charge transfer, which promotes the formation of oxygen vacancies. During methane combustion, gas-phase O_2 is rapidly captured at these vacancies and converted into reactive surface oxygen species (O*),

which oxidize CH_4 directly and at the same time restore the Ni^{3+} and Pd^0 sites consumed in the redox cycle. This also creates new vacancies, resulting in a dynamic equilibrium between vacancies and reactive oxygen species and sustained catalytic activity. Shen et al. [65] demonstrated that the presence of NiO can enhance the re-oxidation ability in the Mars and van Krevelen redox mechanism through the formation of a NiO-PdO alloy structure. Zou et al. [66] studied a series 0.4 wt.% Pd/xNiO/γ-Al_2O_3 with different NiO loading: 0.0, 0.5, 1.0, and 9.0 wt.%. The authors concluded that the interaction between the $NiAl_2O_4$ spinel interface and PdO favoured the distribution of the PdO component, and the formation of well-crystallized PdO, suppressed the PdO particles' aggregation and surface OH^- species accumulation during the reaction, and led to the excellent performance of Pd/0.5NiO/Al_2O_3. The further increasing the spinel $NiAl_2O_4$ amount led to lower activity of the modified catalysts due to greater PdO particle size, lower BET area, and poorer interaction between the spinel $NiAl_2O_4$ and PdO. Y. Liu et. al. [67] showed that the catalyst on well crystallized $NiAl_2O_4$ spinel support exhibited the superior hydrothermal stability. Such excellent catalytic performance has been related to the stabilizing effect of support and the least lattice mismatch between $NiAl_2O_4$ and Pd, which contributed to high Pd dispersion. As noted in the introduction, our previous studies showed that the activity and stability of Pd/Al_2O_3 catalysts in complete methane oxidation are markedly improved by transition metal oxide promoters (Co, Ni, Ce, La) and Co-modified catalysts performed best, owing to the stabilisation of Pd in the active PdO state and the enhanced mobility of lattice oxygen[25–32]. Experimental and theoretical results indicated that the reaction proceeds mainly via a Mars–van–Krevelen mechanism with catalyst reoxidation as the rate-determining step, while the formation of $CoAl_2O_4$ and $NiAl_2O_4$ spinels improved the thermal stability of PdO and the durability of the catalysts.

One possible explanation for the highest activity of the catalyst containing 5 wt% Ni is that it provides the best contact of PdO with nickel aluminate and NiO. In Ni-modified Al_2O_3 at low nickel concentrations, part of the Ni^{2+} initially enters the surface vacancies of γ- Al_2O_3 and forms surface spinel-like Ni^{2+} species [68]. At higher loadings, free NiO, which is reduced at lower temperatures, is also present. This is consistent with our results: the catalysts containing up to 1 wt% Ni show reduction maxima characteristic of finely dispersed NiO and continued reduction above 700 °C, which indicates the formation of a spinel phase. As the nickel content increases, the share of NiO and surface Ni–Al phases also increases. XPS did not detect Co on the surface of the catalysts with nickel content above 1 wt%, which indicates that it is most likely covered by nickel oxide and therefore should not contribute to the catalytic activity. In the remaining samples, cobalt oxide phases are probably accessible and may play a role in stabilising PdO on the surface.

To evaluate the effect of high-temperature calcination, additional experiments were performed using the catalysts with the lowest and the highest nickel contents. Following the deposition of the transition metal species, the samples were calcined according to a three-step procedure: 3 h at 300 °C, 2 h at 450 °C, and 4 h at 800 °C. Palladium was then deposited onto the pre-calcined samples, followed by a final calcination at 450 °C (samples denoted 15Ni+0.5Co (800)+0.2 Pd and 0.25Ni+0.5Co (800)+0.2 Pd).

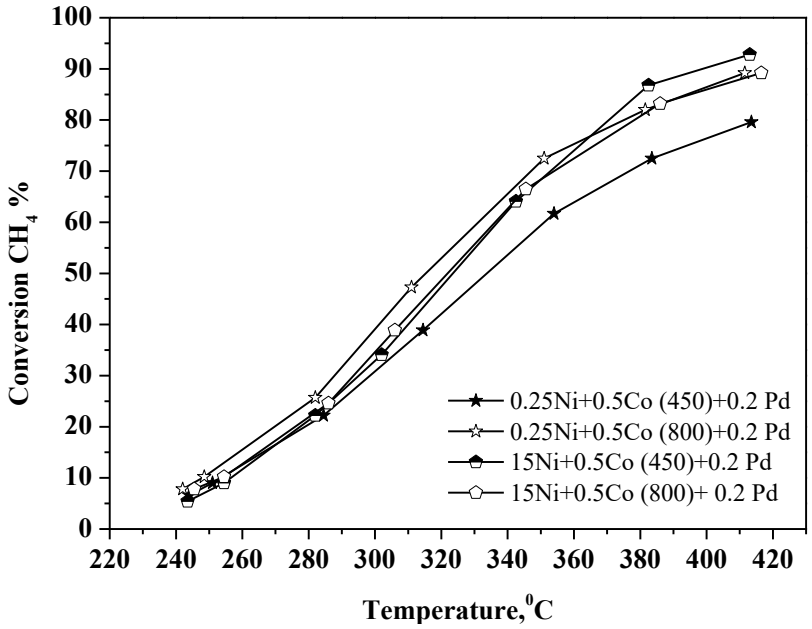


Figure 9. Temperature dependence of methane conversion during complete methane oxidation over xNi+0.5Co +Pd catalysts (x = 0.25 and 15 wt.%) after calcination at different temperatures.

High-temperature calcination at 800 °C enhanced the catalytic activity of the catalyst containing 0.25 wt.% Ni and 0.5 wt.% Co. In contrast, no significant change in catalytic performance was observed for the catalyst containing 15 wt.% Ni, indicating that the calcination temperature applied after the deposition of the transition metal species had little effect on its activity. In contrast, an additional calcination step at 800 °C after palladium deposition resulted in a decrease in catalytic activity for both catalysts investigated. Most likely, the increased activity for the 0.25 wt.% Ni sample is the result of the fact that at high calcination temperature, NiO, which is still present on the support after calcination at 450 °C, interacts with Al_2O_3 and diffuses into its lattice, forming $NiAl_2O_4$. In addition, palladium is present on the surface exclusively in the form of PdO, which is generally considered to be the catalytically active phase in the complete oxidation of methane [26-29].

Conclusions

Several oxide phases are formed on the surface when varying the nickel content during the synthesis of the Pd-Nix-0.5Co/Al_2O_3 catalyst. At nickel contents up to 1 wt%, the main phases are NiO weakly interacting with the support, together with $NiAl_2O_4$ and $CoAl_2O_4$. As the nickel content increases, strongly non-stoichiometric oxide phases appear, consisting of NiO with a moderate interaction with Al_2O_3 and mixed Ni–Al phases.

The simultaneous modification of Al_2O_3 with cobalt and nickel leads to finely dispersed PdO particles that interact only weakly with the support.

Pd^0, Pd^{2+} and Pd^{4+} species are all observed on the surface of the catalysts calcined at 450 °C, whereas calcination of the cobalt- and nickel-modified support at 800 °C results in the formation of aluminate phases on the surface and the stabilisation of palladium as PdO.

The highest activity of the catalyst containing 5 wt% Ni very likely is result of the good contact of PdO with nickel aluminate and NiO. High-temperature calcination at 800 °C

enhanced the catalytic activity of the catalyst with the lowest nickel content, because of the increasing in the nickel aluminate on the surface.

Funding: This work was funded by National Science Fund of Bulgaria grant number КР-06-Н 99/4.

Acknowledgments:

Research equipment of the project № BG16RFPR002-1.014-0006 "National Centre of Excellence Mechatronics and Clean Technologies" was used for experimental work financially supported by European Regional Development Fund under "Research Innovation and Digitization for Smart Transformation" program 2021-2027.

Research equipment from the distributed research infrastructure INFRAMAT (part of the Bulgarian National roadmap for research infrastructures), supported by the Bulgarian Ministry of Education and Science, was also used in the investigation.

Conflicts of interest: The authors have no conflicts of interest to declare that are relevant to the content of this article.

References

1. Wang F, Harindintwali JD, Yuan Z, Wang M, Wang F, Li S, Yin Z, Huang L, Fu Y, Li L, Chang SX, Zhang L, Rinklebe J, Yuan Z, Zhu Q, Xiang L, Tsang DCW, Xu L, Jiang X, Liu J, Wei N, Kästner M, Zou Y, Ok YS, Shen J, Peng D, Zhang W, Barceló D, Zhou Y, Bai Z, Li B, Zhang B, Wei K, Cao H, Tan Z, Zhao LB, He X, Zheng J, Bolan N, Liu X, Huang C, Dietmann S, Luo M, Sun N, Gong J, Gong Y, Brahushi F, Zhang T, Xiao C, Li X, Chen W, Jiao N, Lehmann J, Zhu YG, Jin H, Schäffer A, Tiedje JM, Chen JM. (2021) Technologies and perspectives for achieving carbon neutrality. Innov 2(4):100180. https://doi.org/10.1016/j.xinn.2021.100180

2. Zhang Y, Yan Z, Xiao M, Zhang C, Ruan L, Zhang Y, Zhong Y, Yan Y, Yu Y, He H (2025) Catalytic performance of Pd catalyst supported on CeO_2 or ZrO_2 modified beta zeolite for methane oxidation. J Environ Sci 152:248. https://doi.org/10.1016/j.jes.2024.05.005

3. He L, Fan Y, Bellettre J, Yue J, Luoet L (2020) A review on catalytic methane combustion at low temperatures: Catalysts, mechanisms, reaction conditions and reactor designs. Renew Sustain Energy Rev 119:109589. https://doi.org/10.1016/j.rser.2019.109589

4. Mortensen RL, Noack H-D, Pedersen K, Mossin S, Mielbyet J (2022) Recent Advances in complete methane oxidation using zeolite-supported metal nanoparticle catalysts. ChemCatChem 14(16):e202101924. https://doi.org/10.1002/cctc.202101924

5. Chen J, Arandiyan H, Gao X, Li J (2015) Recent advances in catalysts for methane combustion. Catal Surv Asia 19:140-171. https://doi.org/10.1007/s10563-015-9191-5

6. Arendt E, Maione A, Klisinska A, Sanz O, Montes M, Suarez S, Blanco J, Ruiz P. (2009) Structuration of Pd (2 wt %)/Fe−Al Oxide Catalysts on Ceramic and Metallic Monoliths: Physicochemical Characterization, Effect of the Nature of the Slurry, and Comparison with $LaMnO_3$ Catalysts. J Phys Chem C 113:16503-16516. https://doi.org/10.1021/jp901056z

7. US Environmental Protection Agency (2013) 2013 Revisions to the greenhouse gas reporting rule and proposed confidentiality determinations for new or substantially revised data elements, 40 CFR Part 98. Fed Regist 78(63), 2 April 2013 (Proposed Rules)

8. United Nations Environment Programme. https://www.unep.org/news-and-stories/story/new-global-methane-pledge-aims-tackle-climate-change

9. Feng X, Jiang L, Li D, Tian S, Zhu X, Wang H, He C, Li K (2022) Progress and key challenges in catalytic combustion of lean methane. J Energy Chem 75:173-215. https://doi.org/10.1016/j.jechem.2022.08.001

10. European Parliament and Council of the European Union (2024) Regulation (EU) 2024/1787 of 13 June 2024 on the reduction of methane emissions in the energy sector and amending Regulation (EU) 2019/942

11. Rotko M, Machocki A, Stasinska B (2010) Studies of catalytic process of complete oxidation of methane by SSITKA method. Appl Surf Sci 256:5585-5589. https://doi.org/10.1016/j.apsusc.2009.12.152

12. Specchia S, Finocchio E, Busca G, Palmisano P, Specchia V (2009) Surface chemistry and reactivity of ceria–zirconia-supported palladium oxide catalysts for natural gas combustion. J Catal 263:134-145. https://doi.org/10.1016/j.jcat.2009.02.002

13. Raj A (2016) Methane Emission Control A review of mobile and stationary source emissions abatement technologies for natural gas engines. Johnson Matthey Technol Rev 60:228-235. https://doi.org/10.1595/205651316X692554

14. Monai M, Montini T, Gorte RJ, Fornasiero P (2018) Catalytic oxidation of methane: Pd and beyond. Eur J Inorg Chem 2018:2884-2893. https://doi.org/10.1002/ejic.201800326

15. Y Wu, Li G, Hu W, Huang F, Chen J, Zhong L, Chen Y (2018) Effect of MOx (M = Ce, Ni, Co, Mg) on activity and hydrothermal stability of Pd supported on ZrO_2–Al_2O_3 composite for methane lean combustion. J Taiwan Inst Chem Eng 85:176-185. https://doi.org/10.1016/j.jtice.2018.01.038

16. Liotta LF, Carlo D, Pantaleo G, Venezia A.M, Deganello G, Merlone Borla E, Pidria M (2007) Combined CO/CH_4 oxidation tests over Pd/Co_3O_4 monolithic catalyst: Effects of high reaction temperature and SO_2 exposure on the deactivation process. Appl Catal B 75:182-188. https://doi.org/10.1016/j.apcatb.2007.04.012

17. Qiao D, Lu G, Mao D, Liu X, Li H, Guo Y, Guo Y (2010) Effect of Ca doping on the catalytic performance of CuO–CeO_2 catalysts for methane combustion. Catal Commun 11:858-861. https://doi.org/10.1016/j.catcom.2010.03.010

18. Li J, Liang X, Xu S, Hao J (2009) Catalytic performance of manganese cobalt oxides on methane combustion at low temperature. Appl Catal B 90:307-312. https://doi.org/10.1016/j.apcatb.2009.03.027

19. Ren XG, Zheng JD, Song YJ (2011) Effects of different ion doping on the structure and methane combustion performance of lanthanum hexaaluminate catalysts. J Fuel Chem Technol 39:717-720.

20. Sekizawa K, Eguchi K, Widjaja H, Machida, M, Arai H (1996) Property of Pd-supported catalysts for catalytic combustion. Catal Today 28:245-250. https://doi.org/10.1016/0920-5861(95)00241-3

21. Widjaja H, Sekizawa K, Eguchi K, Arai H. (1999) Oxidation of methane over Pd/mixed oxides for catalytic combustion. Catal Today 47:95-101. https://doi.org/10.1016/S0920-5861(98)00286-7

22. Thevenin PO, Alcalde A, Pettersson LJ, Järås S G, Fierro J LG (2003) Catalytic combustion of methane over cerium-doped palladium catalysts. J Catal 215:78-86. https://doi.org/10.1016/S0021-9517(02)00146-X

23. Wang B, Qin Z, Wang G, Wu, Z, Fan W, Zhu H, Li S, Zhang Y, Li Z, Wang J (2013) Catalytic combustion of lean methane at low temperature over palladium on a CoOx –SiO_2 composite support. Catal Lett 143:411-417. https://doi.org/10.1007/s10562-013-0988-4

24. Yu Y, Takei T, Ohashi H, He H, Zhang X, Haruta M. (2009) Pretreatments of Co_3O_4 at moderate temperature for CO oxidation at −80 °C. J Catal 267(2):121-128. https://doi.org/10.1016/j.jcat.2009.08.003

25. Todorova S, Stefanov P, Naydenov A, Kolev H (2014) Catalytic oxidation of methane over Pd–MeOx (Me = Mn, Co, Ni, Ce) catalysts — influence of metal oxides. Rev Roum Chim 59(3-4):251-257.

26. Stefanov P, Todorova S, Naydenov A, Tzaneva B, Kolev H, Atanasova G, Stoyanova D, Karakirova Y, Aleksieva K. (2015) On the development of active and stable Pd–Co/γ-Al_2O_3 catalyst for complete oxidation of methane Chem Eng J 266:329. https://doi.org/10.1016/j.cej.2014.12.099

27. Tzaneva B, Naydenov A, Todorova S, Videkova V.H., Milusheva VS, P K Stefanov (2016) Cobalt electrodeposition in nanoporous anodic aluminium oxide for application as catalyst for methane combustion. Electrochim Acta 191:192-199. https://doi.org/10.1016/j.electacta.2016.01.063

28. Todorova S, Naydenov A, Kolev H, Larin, A, Tenchev, K. (2018) Catalytic oxidation of methane over co modified Pd/Al_2O_3 catalysts – influence of the cobalt loading Int J Adv Sci Eng Technol 6(3):64-69.

29. Todorova S, Naydenov A, Velinova R, Kolev H, Larin·A V, Stoyanova D, · Shopska M,· Tenchev K,· Stefanov P (2019) Pd–MeOx/Al_2O_3 (Me = Co, La, Ce) catalysts for methane combustion. React Kinet Mech Catal 126:663-678. https://doi.org/10.1007/s11144-018-1523-9

30. Velinova R, Todorova S, Drenchev B, Ivanov G, Shipochka M, Markov P, Nihtianova D, Kovacheva D, Larin AV, Naydenov A (2019) Complex study of the activity, stability and sulfur resistance of Pd/La_2O_3-CeO_2-Al_2O_3 system as monolithic catalyst for abatement of methane Chem Eng J 368:865-876. https://doi.org/10.1016/j.cej.2019.03.017

31. Todorova S, Naydenov A, Velinova R, Kolev H, Larinc, Karashanova D (2022) Catalytic combustion of methane over Ni modified Pd/Al_2O_3 catalysts. Mater Today Proc 61:1212-1216. https://doi.org/10.1016/j.matpr.2022.01.267

32. Rybakov AA, Bryukhanov IA, Todorova S, Velinova R, Naydenov A, Larinl A V, (2020) Spatial and Magnetic Factors for CH_4 Oxidation on Pd Slabs in the Presence of Transition-Metal Me Cations Exchanged in γ-Al_2O_3 Support or $MeAl_2O_4$ Spinels, Me = Ni, Co, Mn J Phys Chem C 124(1):605. https://doi.org/10.1021/acs.jpcc.9b09400

33. Li Y, Hasin P, Wu Y (2010) $Ni_xCo_{3-x}O_4$ Nanowire arrays for electrocatalytic oxygen evolution. Adv Mater 22(17):1926-1929. https://doi.org/10.1002/adma.200903896

34. Tao FF, Shan J-J, Nguyen L, Wang Z, Zhang S, Zhang L, Wu Z, Huang W, Zeng S, Hu P (2015) Understanding complete oxidation of methane on spinel oxides at a molecular level. Nat Commun 6:7798. https://doi.org/10.1038/ncomms8798

35. Trivedi S, Prasad R, Gautam SK (2018) Design of active $NiCo_2O_{4-\delta}$ spinel catalyst for abatement of CO-CH_4 emissions from CNG fueled vehicles. AIChE J 64:2632. https://doi.org/10.1002/aic.16162

36. Shirley DA (1972) High-resolution x-ray photoemission spectrum of the valence bands of gold. Phys Rev B 5(12):4709-4714. https://doi.org/10.1103/PhysRevB.5.4709

37. Scofield JH (1976) Hartree-Slater subshell photoionization cross-sections at 1254 and 1487 eV. J Electron Spectrosc Relat Phenom 8(2):129-137. https://doi.org/10.1016/0368-2048(76)80015-1

38. Thommes M, Kaneko K, Neimark AV, Olivier JP, Rodriguez-Reinoso F, Rouquerol J, Sing KSW (2015) Physisorption of gases, with special reference to the evaluation of surface area and pore size distribution (IUPAC Technical Report). Pure Appl Chem 87:1051-1069. https://doi.org/10.1515/pac-2014-1117

39. Siang TJ, Singh S, Omoregbe O, Bach L G, Phuc N H H, Vo D-V N. (2018) Hydrogen production from CH_4 dry reforming over bimetallic Ni–Co/Al_2O_3 catalyst. J Energy Inst 91:683-694. https://doi.org/10.1016/j.joei.2017.06.001

40. Liu C, Hou R, Wang T (2015) Role of acid sites and surface hydroxyl groups in isophthalonitrile hydrogenation catalyzed by supported Ni–Co catalysts. RSC Adv 5:26465. https://doi.org/10.1039/c5ra01007a

41. Luo MF, Zheng XM (1999) Redox behaviour and catalytic properties of $Ce_{0.5}Zr_{0.5}O_2$-supported palladium catalysts. Appl Catal A 189:15-21. DOI: 10.1016/S0926-860X(99)00230-6

42. Zhou R, Zhao B, Yue B (2008) Effects of CeO_2-ZrO_2 present in Pd/Al_2O_3 catalysts on the redox behavior of PdOx and their combustion activity. Appl Surf Sci 254:4701-4707. https://doi.org/10.1016/j.apsusc.2008.01.075

43. Kwon Y, Eichler JE, Mullins CB (2022) $NiAl_2O_4$ as a beneficial precursor for Ni/Al_2O_3 catalysts for the dry reforming of methane. J CO2 Util 63:102112. https://doi.org/10.1016/j.jcou.2022.102112

44. Gabrovska MV, Edreva-Kardjieva RM, Crişan DD, Tenchev K K, Nikolova D A, Crişan M (2013) Structure and reducibility of the mixed metal oxides obtained from Ni–Al layered double hydroxides. Catalytic activity in CO_2 methanation reaction. Bulg Chem Commun 45:617-624

45. Zhou L, Li L, Wei N Li J, Basset J-M (2015) Effect of $NiAl_2O_4$ formation on Ni/Al_2O_3 stability during dry reforming of methane. ChemCatChem 7:2508-2516. https://doi.org/10.1002/cctc.201500379

46. Arnoldy P, Moulijn JA (1985) Temperature-programmed reduction of CoO/Al_2O_3 catalysts. J Catal 93:38-54. https://doi.org/10.1016/0021-9517(85)90149-6

47. Nyathi TM, Fischer N, York APE, Morgan DJ, Hutchings GJ, Gibson E K, Wells P P Catlow CR A, Claeys M. (2019) Impact of nanoparticle–support interactions in Co_3O_4/Al_2O_3 catalysts for the preferential oxidation of carbon monoxide. ACS Catal 9(8):7166-7178. https://doi.org/10.1021/acscatal.9b00685

48. Chen T, Li W, Yu C, Jin R, Xu H (2000) The importance of nonstoichiometric oxygen in NiO for the catalytic oxidative dehydrogenation of ethane. Stud Surf Sci Catal 130:1847-1852. https://doi.org/10.1016/S0167-2991(00)80470-X

49. Iwamoto M, Yoda Y, Egashira M, Egashira M, Seiyama T (1976) Study of metal oxide catalysts by temperature programmed desorption. 1. Chemisorption of oxygen on nickel oxide. J Phys Chem 80:1989-1994. https://doi.org/10.1021/j100559a008

50. Dubey P, Kaura N, Devan RS, Okram GS, Kuo YK (2018) The effect of stoichiometry on the structural, thermal and electronic properties of thermally decomposed nickel oxide. RSC Adv 8:5882-5890. https://doi.org/10.1039/C8RA00157J

51. Todorova S, Blin JL, Naydenov A, Lebeau B, Kolev H, Gaudin P, Dotzeva A, Velinova R, Filkova D, Ivanova I, Vidal L, Michelin L, Josien L, Tenchev K (2020) Co_3O_4-MnOx oxides supported on SBA-15 for CO and VOCs oxidation. Catal Today 357:602-612. https://doi.org/10.1016/j.cattod.2019.05.018

52. Pinaeva LG, Prosvirin IP, Dovlitova LS, Danilova IG, Sadovskaya E M, Isupova L A (2016) MeOx/Al_2O_3 and MeO_x/CeO_2 (Me = Fe, Co, Ni) catalysts for high temperature N_2O decomposition and NH_3 oxidation. Catal Sci Technol 6:2150. https://doi.org/10.1039/c5cy01381j

53. Nandi P, Park H, Shin S, Lee J-W, Kim J Y, Ko M J, Jung H S, Park N-G, Shin H (2024) NiO as hole transporting layer for inverted perovskite solar cells: a study of X-ray photoelectron spectroscopy. Adv Mater Interfaces. https://doi.org/10.1002/admi.202300751

54. Horsth DFL, Primo JDO, Balaba N, Anaissi F J, Bittencourt C (2023) Color stability of blue aluminates obtained from recycling and applied as pigments. RSC Sustain 1:159-166. https://doi.org/10.1039/D2SU00057A

55. Jiménez-González C, Boukha Z, de Rivas B, Delgado J J, Cauqui M Á, González-Velasco JR, Gutiérrez-Ortiz J I, López-Fonseca R (2013) Structural characterisation of Ni/alumina reforming catalysts activated at high temperatures. Appl Catal A Gen 466:9-20. https://doi.org/10.1016/j.apcata.2013.06.017

56. Natile MM, Glisenti A (2002) Surface reactivity of NiO: interaction with methanol. Chem Mater 14:4895-4903. https://doi.org/10.1021/cm0211047

57. Heracleous E, Lee AF, Wilson K, Lemonidou A A (2005) Investigation of Ni-based alumina-supported catalysts for the oxidative dehydrogenation of ethane to ethylene: structural characterization and reactivity studies. J Catal 231:159-171. https://doi.org/10.1016/j.jcat.2005.01.015

58. Thermo Fisher Scientific, XPS periodic table. Thermo Fisher Scientific – XPS (accessed 1 September 2026)

59. Pei A, Wang P, Zhang S (2024) Enhanced electrocatalytic biomass oxidation at low voltage by Ni^{2+}–O–Pd interfaces. Nat Commun 15:5899. https://doi.org/10.1038/s41467-024-50325-w

60. Liu Z, Guan T, Sun H, Lu X, Zhou P, Liu Y, Chen Y, Zhu J-J, Zhang J-R, Zhu W (2026) Precisely modulating the interfacial oxygen radicals for selective photocatalytic methane partial oxidation to methanol. Angew Chem Int Ed 65(29):e1583650. https://doi.org/10.1002/anie.1583650

61. He L, Ren Y, Yue B, Tsang S C E, He H (2021) Tuning metal–support interactions on Ni/Al_2O_3 catalysts to improve catalytic activity and stability for dry reforming of methane. Processes 9:706. https://doi.org/10.3390/pr9040706

62. Moulder JF, Stickle WF, Sobol PE, Bomben KD (1992) Handbook of X-ray photoelectron spectroscopy: a reference book of standard spectra for identification and interpretation of XPS data. Chastain J (ed) Perkin-Elmer Corporation, Physical Electronics Division, Eden Prairie

63. Chin RL, Hercules DM (1982) Surface spectroscopic characterization of cobalt-molybdenum-alumina catalysts. J Phys Chem 86:3079-3089. https://doi.org/10.1021/j100213a008

64. Li J, Yang J, Zhu L, Sun S, Chen X, Liu X, Xu F (2025) Morphology-dependent activity of Pd/NiO catalysts for low-concentration methane combustion. Results Chem 18:102812. https://doi.org/10.1016/j.rechem.2025.102812

65. Shen J, Hayes RE, Wu X, Semagina N (2015) 100° Temperature reduction of wet methane combustion: highly active $Pd\text{-}Ni/Al_2O_3$ catalyst versus $Pd/NiAl_2O_4$. ACS Catal 5:2916-2920. https://doi.org/10.1021/acscatal.5b00060

66. Zou X, Rui Z, Song S, Ji H (2016) Enhanced methane combustion performance over $NiAl_2O_4$-interface-promoted $Pd/\gamma\text{-}Al_2O_3$. J Catal 338:192-201. https://doi.org/10.1016/j.jcat.2015.12.031

67. Liu Y, Wang S, Sun T, Gao D, Zhang C, Wang S (2012) Enhanced hydrothermal stability of high performance lean fuel combustion alumina-supported palladium catalyst modified by nickel. Appl Catal B 119-120:321-328. https://doi.org/10.1016/j.apcatb.2012.02.032

68. Garbarino G, Riani P, Infantes-Molina A, Rodríguez-Castellón E, Busca G (2016) On the detectability limits of nickel species on $NiO/\gamma\text{-}Al_2O_3$ catalytic materials. Appl Catal A 525:180-189. https://doi.org/10.1016/j.apcata.2016.07.017